ELSEVIER

Journal of Structural Geology 26 (2004) 1677–1692

JOURNAL OF STRUCTURAL GEOLOGY

www.elsevier.com/locate/jsg

Mullions in the High-Ardenne Slate Belt (Belgium): numerical model and parameter sensitivity analysis

I. Kenis[a,*], J.L. Urai[b], W. van der Zee[b,c], M. Sintubin[a]

[a]*Structural Geology & Tectonics Group, Katholieke Universiteit Leuven, Redingenstraat 16, 3000 Leuven, Belgium*
[b]*Geologie-Endogene Dynamik, RWTH Aachen, Lochnerstrasse 4-20, 52056 Aachen, Germany*
[c]*Now at: GeoMechanics International, Mainz, Germany*

Received 4 March 2003; received in revised form 13 January 2004; accepted 2 February 2004

Available online 19 March 2004

Abstract

In the High-Ardenne Slate Belt (Belgium), pre-existing layer-perpendicular quartz veins in psammite layers acted as mechanical boundaries due to the difference in competence between vein quartz and psammite. This caused the formation of mullions during layer-parallel shortening. In this paper, the process of mullion formation is modelled using finite-element techniques. A parameter sensitivity analysis of the mullion model demonstrates that the stress exponent of psammite, the total horizontal shortening of the psammite layers, the initial aspect ratio of the psammite segments between the veins and the competence contrast between psammite and vein quartz are the controlling parameters for the shape of the mullions. Our results suggest that the morphology of the mullions can be used to constrain the rheology of psammite deforming in the middle crust. Moreover, the parameter sensitivity analysis illustrates the range of layer-parallel shortening/extension structures associated with layer-perpendicular quartz veins that can be expected in nature (e.g. dogbones, inverted mullions) and creates future perspective for the use of the model as a paleorheological gauge for these structures.

Keywords: Mullions; Quartz veins; Finite elements; Rheology

1. Introduction

Many recent developments in our understanding of deformation in the Earth's crust come from geodynamic models. Such models incorporate the geometries, boundary conditions and rock rheologies in the subsurface. Unfortunately, the rheology of rocks deforming under natural conditions is poorly known. Modellers commonly use generic viscosity contrasts or laboratory-derived flow laws under the assumption that they can be extrapolated over several orders of magnitude to geological conditions (e.g. Cattin and Avouac, 2000). An olivine-controlled rheology is commonly assumed for the upper mantle (Jackson, 2002), whereas the ductile parts of the crust are modelled using power-law creep equations describing crystal–plastic flow of quartz or feldspar (Bos and Spiers, 2002). Lithospheric strength profiles are based on flow laws for monomineralic materials obtained from relatively low-strain experiments. Kohlstedt et al. (1995) suggested that flow strengths predicted from laboratory data probably overestimate the actual rock strength. In dislocation creep mode, the weakest phase probably dominates rock behaviour (Burov, 2003) and is not necessarily quartz. Very weak phases can be e.g. albite or micas. Depending on microstructure and composition, polyphase quartz-rich rocks may be significantly weaker than pure quartz (Bos and Spiers, 2002). In summary, the long-term rheological behaviour of the crust and mantle are not well known and subject of recent controversy (Jackson, 2002; Burov, 2003; Ranalli, 2003). Based on field data, attempts have been made to constrain viscosity contrast between different rocks that were reviewed by Talbot (1999). Biot (1961) related the ratio of dominant wavelength to the thickness of buckled competent layers to the ratio of the viscosity of the layer to its host rock. Treagus (1983, 1988) used the cleavage refraction angle between competent and incompetent materials to estimate the ratio of their effective viscosities. Strain variations among the component rock fragments of

* Corresponding author. Tel.: +32-16-326448; fax: +32-16-326401.
E-mail address: ilse.kenis@geo.kuleuven.ac.be (I. Kenis).

0191-8141/$ - see front matter © 2004 Elsevier Ltd. All rights reserved.
doi:10.1016/j.jsg.2004.02.001

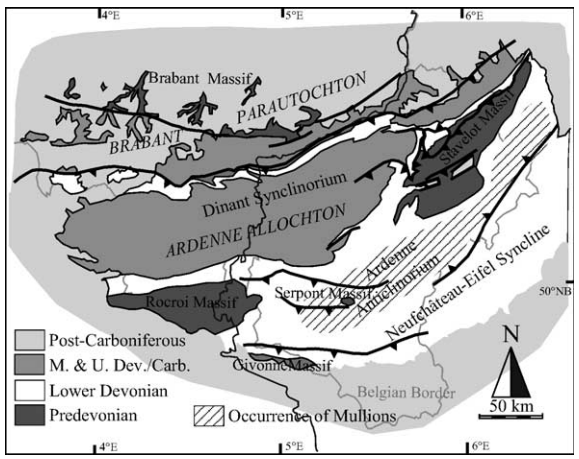

Fig. 1. Geological map of the High-Ardenne Slate Belt (Belgium), showing the zone of occurrence of the mullions. The High-Ardenne Slate Belt is composed of the Ardenne Anticlinorium and the Neufchâteau–Eifel Syncline, which predominantly consist of Lower Devonian metasedimentary sequences.

conglomerates were used to quantify the effective viscosity ratios (Treagus and Treagus, 2002).

The aim of this paper is to contribute to solving this problem. The approach is to model the evolution of mullions associated with quartz veins using finite-element techniques. We present a parameter sensitivity analysis of the numerical mullion model, which demonstrates the effect of the different geological parameters on the resulting shape of the mullions. The analysis also illustrates the range of layer-parallel shortening/extension structures associated with layer-perpendicular quartz veins that can be expected in the field. We moreover explore the possible use of mullions to constrain paleorheology.

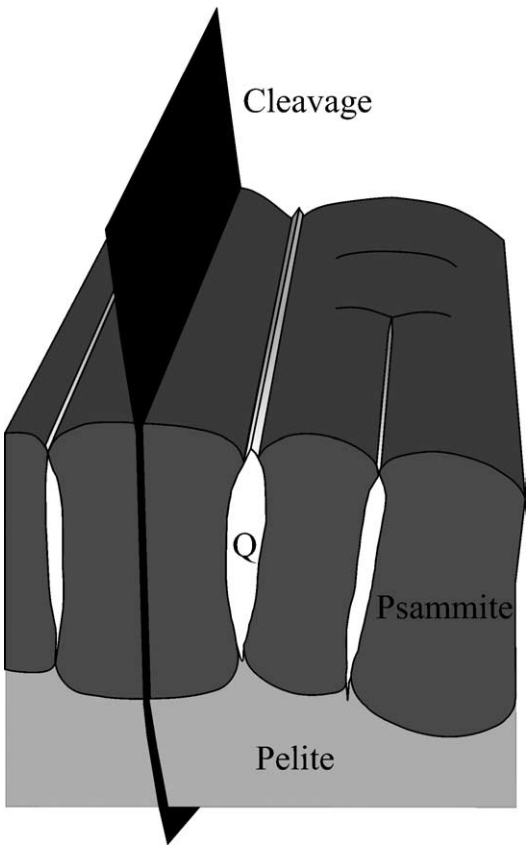

Fig. 2. Schematic drawing of a series of mullions. Q = quartz (not to scale).

2. Geological setting

Mullions associated with quartz veins frequently occur in the High-Ardenne Slate Belt (Fig. 1). This slate belt predominantly consists of siliciclastic, metasedimentary sequences of early Devonian age, which underwent a low-grade, burial to early-synkinematic, metamorphism (Beugnies, 1983; Fielitz and Mansy, 1999). This metamorphic event is interpreted to be younger than some magmatic intrusions in the Lower Palaeozoic basement, which are dated at 373 and 381 Ma (Kramm and Buhl, 1985; Goffette et al., 1991; Fielitz and Mansy, 1999).

The mullions are characterised by a cylindrical cuspate–lobate geometry of the pelite–psammite interface, separated by lensoid quartz veins that are oriented at high angle to the bedding (Fig. 2). Describing these structures, Lohest et al. (1908) for the first time used the terms ‘boudin’ and ‘boudinage’. Recently, a new dynamic model for the development of these structures was independently and simultaneously proposed by Urai et al. (2001) and Kenis et al. (2002) (Fig. 3). This model is briefly summarized below.

Hydraulic fracturing in regional high-pressure compartments was responsible for the formation of the veins (Kenis et al., 2002). Kenis et al. (2002) proposes that these veins formed in low-grade metamorphic conditions at maximum burial depth (~10 km). Coexisting, syngenetic aqueous and gaseous fluid inclusions of the vein quartz and chlorite geothermometry show that the veins formed at a temperature of ~350–400 °C (Darimont et al., 1988; Verhaert, 2001).

Layer-parallel shortening during the early stage of the Late Palaeozoic Variscan orogeny acted on psammite layers containing the quartz veins. The veins acted as mechanical boundaries due to their difference in competence with respect to the psammite (Urai et al., 2001; Kenis et al., 2002). This resulted in buckling of the interface between pelite and psammite and thus the formation of mullions (Fig. 3). Given the fact that there was only a small discrepancy in time between the formation of the veins and mullions, similar temperature conditions are assumed for both events.

Variscan horizontal shortening started in the early Viséan (335–330 Ma; Oncken et al., 1999, 2000). Deformation was intensified when the Variscan deformation front propagated through the Devono-Carboniferous basin fill between 325 and 300 Ma ago (Ahrendt et al., 1983), with cleavage development and folding between 325 and 310 Ma ago. Taking into account the kinematic constraints of Kenis et al.

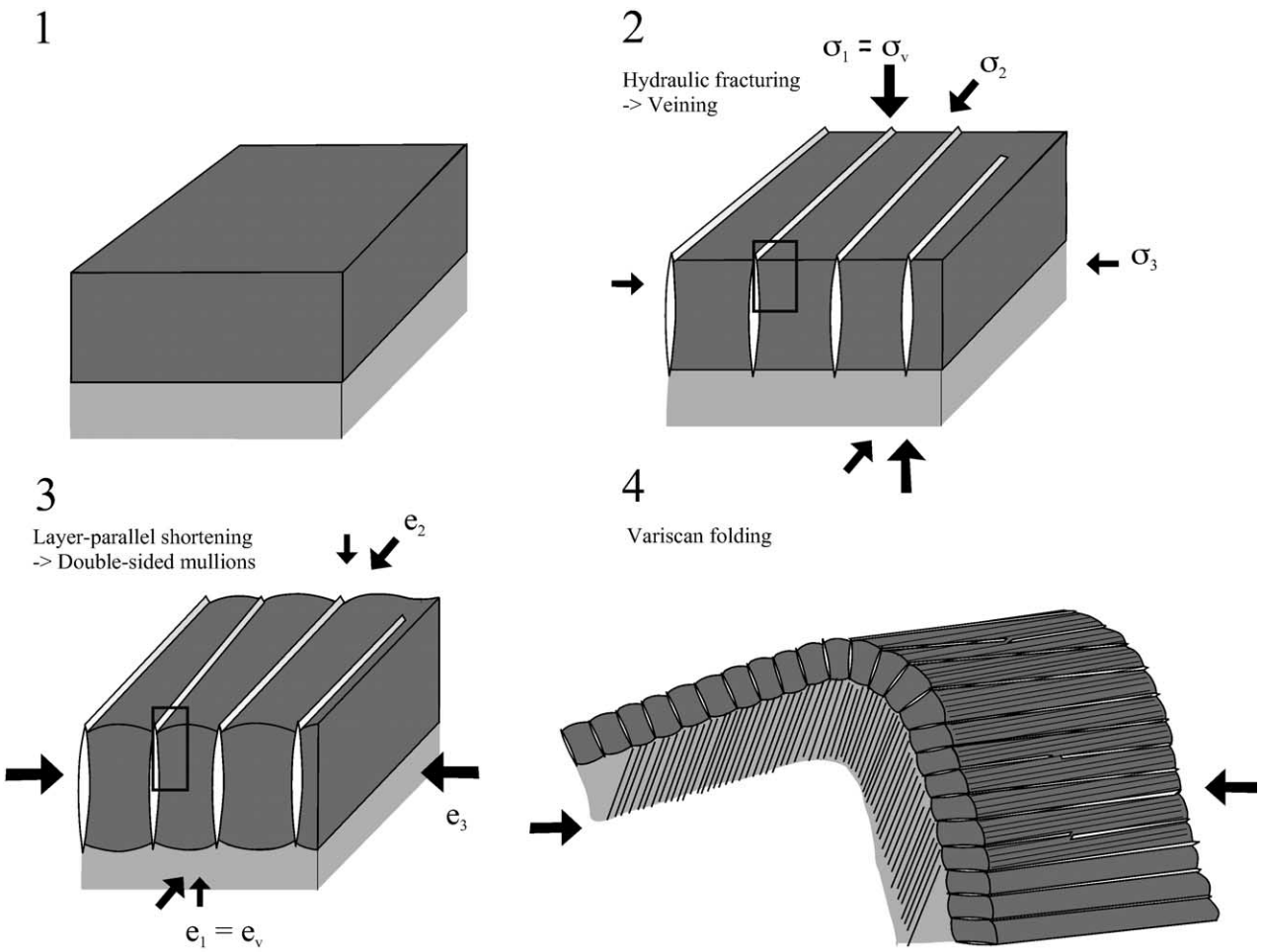

Fig. 3. Polyphase deformation model for the development of the mullions in the High-Ardenne Slate Belt (after Kenis et al., 2002). (1) Layer configuration during sedimentation and first stages of burial. (2) Hydraulic fracturing during latest stages of burial enables formation of quartz veins. (3) Mullion development due to layer-parallel shortening at the onset of the Variscan deformation. (4) Variscan cleavage- and folding development due to progressive deformation. The dark grey square in (2) and (3) correspond to the discretised part of the mullion model (see also Figs. 4 and 5).

(2002), the longest period available for mullion development is therefore estimated at 10 Ma (from 335 to 325 Ma).

Urai et al. (2001) and Kenis et al. (2002) also discussed the nomenclature relating to these structures, which were initially called 'boudins' (Lohest et al., 1908). In current usage, boudins formed by the process of layer-parallel extension of competent layers enclosed in a less competent matrix. Mullions are cusp-like corrugations at the interface of units of different competencies in a multilayer sequence affected by layer-parallel shortening. Based on these kinematic definitions, Kenis et al. (2002) and Urai et al. (2001) postulate that the structures in the High-Ardenne Slate Belt should be termed mullions at both interfaces bounded by veins ('double-sided mullions').

3. Mullion model

A simplified analytic model (Urai et al., 2001) suggests that the morphology of the mullions is a strong function of the stress exponent of the power-law creep equation of psammite. In this study, we present a more representative numerical model using finite-element techniques, which takes into account the geological boundary conditions discussed above.

We use a viscoplastic formulation in which the strain-rate potential can be written as a function of equivalent stress, as implemented in the ABAQUS software package (Hibbitt et al., 2002). The model consists of four parts: (1) the mesh generation, (2) the material properties, (3) the boundary conditions, and (4) the history information.

3.1. Mesh generation and boundary conditions

We simplify the modelling based on the near-orthorhombic symmetry of the mullions (Fig. 3). Therefore only 1/2nd of a mullion at a psammite–pelite interface is discretised, reducing the computation time. We assume plane strain (cf. Fletcher, 1995). This assumption is justified for mullions where the bedding–cleavage intersection is parallel to the mullion axis (see Urai et al., 2001; Kenis et al., 2002).

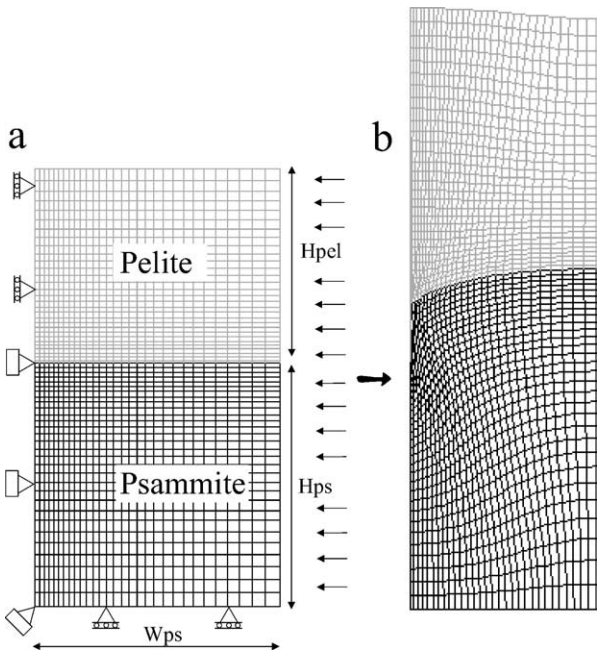

Fig. 4. Mesh of model 1. The triangles give a representation of the boundary conditions imposed on the model. *H* pel—height pelite, *W* ps—width psammite, *H* ps—height psammite.

Two models were developed to perform the parameter sensitivity analysis (Figs. 4 and 5). The first model assumes a fully rigid, infinitesimally thin vein (rigid vein model 1; Fig. 4). This configuration is simulated by imposing no vertical or horizontal displacement on the lower left side of the grid (corresponding to the psammite). On the lower side of the grid no vertical displacement is imposed, while the top left side of the grid (corresponding to the pelite) is only restricted in the horizontal direction (Fig. 4). The top side of the grid is free and a horizontal displacement is imposed on the right side of the model.

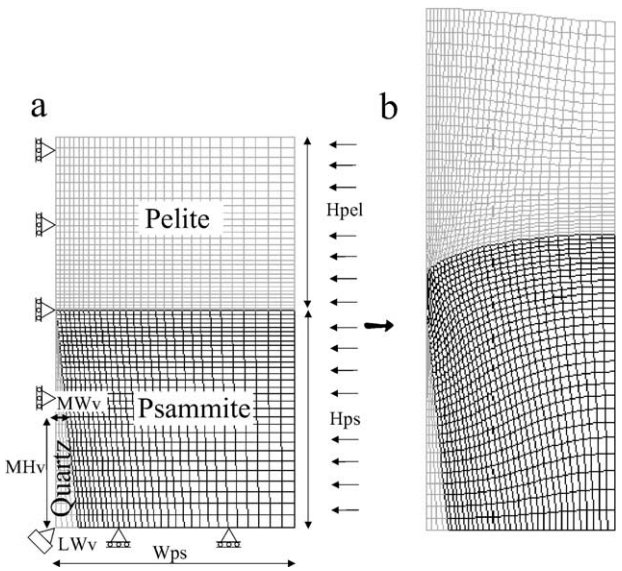

Fig. 5. Mesh of model 2. The triangles give a representation of the boundary conditions imposed on the model. *H* pel—height pelite, *W* ps—width psammite, *H* ps—height psammite, *MH* v—mid-height vein, *MW* v—mid-width vein, *LW* v—lower-width vein.

The second model is an extension of the first model and represents the full configuration including a vein (model 2; Fig. 5). In this model, only the left side of the mesh is fixed in the horizontal direction and the lower side of the mesh is fixed in the vertical direction (Fig. 5).

We start both models with a homogeneous stress state. This is justified by the fact that after deep burial, at the onset of the Variscan deformation, the rocks have to go through a near-isotropic stress state (Kenis et al., 2002). This isotropic stress state comes from an inversion of σ_1 and σ_3 during the transition of the burial state to horizontal compression due to the Variscan orogeny (Fig. 3).

Microscopic observations indicate that the strain in the mullions is largest at the tip of the vein. This can be explained considering the elastic stresses at the tip of the vein in both models, which are singular in a crack-like way (Timoshenko and Goodier, 1970; Rudnicki, pers. comm.). That is, the stresses in the neighbourhood of the tip of the vein are proportional to the $(\text{radius})^{(-1/2)}$, where the radius is the distance to the tip of the vein. At the onset of the deformation this will lead to high strain rates and redistribution of stress in this region, and this process is not accurately described using the discretisation we used. However, using models with different mesh refinements it was shown that this leads to errors in a very small area around the tip of the vein and displacements in the rest of the model are not affected. Therefore, in the present analysis we did not use results in this small area; detailed analysis of the strains and microstructures in the cusp will be presented in the future.

3.2. Material properties

In both models, a volume-constant steady-state power-law creep rheology is assumed for the three materials: vein quartz, psammite and pelite. This flow law is generally used to describe the macroscopic rheology for silicates in the crust below the brittle–ductile transition and has the form (Weertman, 1968):

$$\delta\epsilon/\delta t = A_0(\sigma_1 - \sigma_3)^n \exp^{(-Q/RT)} d^{-m} \quad (1)$$

where $\delta\epsilon/\delta t$ is the strain rate, A_0 is a material constant, $\sigma_1 - \sigma_3$ is the differential stress, n the stress exponent, Q the activation enthalpy, R the gas constant, T the temperature, d the grain size and m the grain size exponent (cf. Heard and Carter, 1968; Parrish et al., 1976; Shelton and Tullis, 1981; Jaoul, 1984; Jaoul et al., 1984; Kronenberg and Tullis, 1984; Koch et al., 1989; Paterson and Luan, 1990; Luan and Paterson, 1992; Gleason and Tullis, 1995; Hirth et al., 2001).

In ABAQUS the power-law creep equation is written as:

$$\delta\epsilon/\delta t = A(\sigma_1 - \sigma_3)^n t^m \quad (2)$$

where $\delta\epsilon/\delta t$ is the strain rate, A the material constant

Table 1
Table of input parameters for the different models used in the parameter sensitivity analysis. W = width; H = height; LW = lower width; MW = middle width; MH = middle height; ps = psammite; pel = pelite; v = vein; qtz = quartz; E = Young's modulus; ν = poisson ratio; A (see Eq. (2) in text); n = stress exponent of power law equation; t.o.d. = time of deformation; displ = displacement. See also Fig. 5

Label input file	W ps	H ps	H pel	LW v	MW v	MH v	E ps	ν ps	A ps	n ps	E pel	ν pel	A pel	n pel	E qtz	ν qtz	A qtz	n qtz	t.o.d.	displ
A 2.1×10^{-22} = 25% = n4	50	50	90				$1\times10^{+05}$	0.28	1.12×10^{-21}	4	$1\times10^{+05}$	0.26	1.12×10^{-21}	4					$3.0\times10^{+14}$	−12.5
A 3.02×10^{-23}	50	50	90				$1\times10^{+05}$	0.28	7.76×10^{-21}	4	$1\times10^{+05}$	0.26	7.76×10^{-21}	4					$3.0\times10^{+14}$	−12.5
A 1×10^{-35}	50	50	90				$1\times10^{+05}$	0.28	1.00×10^{-35}	4	$1\times10^{+05}$	0.26	1.00×10^{-35}	4					$3.0\times10^{+14}$	−12.5
5%	50	50	90				$1\times10^{+05}$	0.28	1.12×10^{-21}	4	$1\times10^{+05}$	0.26	1.12×10^{-21}	4					$3.0\times10^{+14}$	−2.5
10%	50	50	90				$1\times10^{+05}$	0.28	1.12×10^{-21}	4	$1\times10^{+05}$	0.26	1.12×10^{-21}	4					$3.0\times10^{+14}$	−5
40%	50	50	90				$1\times10^{+05}$	0.28	1.12×10^{-21}	4	$1\times10^{+05}$	0.26	1.12×10^{-21}	4					$3.0\times10^{+14}$	−20
20% extension	50	50	90				$1\times10^{+05}$	0.28	1.12×10^{-21}	4	$1\times10^{+05}$	0.26	1.12×10^{-21}	4					$3.0\times10^{+14}$	20
pel 4/5 = psam 1/1	50	50	90				$1\times10^{+05}$	0.28	1.12×10^{-21}	4	$1\times10^{+05}$	0.26	1.12×10^{-21}	4					$3.0\times10^{+14}$	−12.5
pel 2/5	50	50	70				$1\times10^{+05}$	0.28	1.12×10^{-21}	4	$1\times10^{+05}$	0.26	1.12×10^{-21}	4					$3.0\times10^{+14}$	−12.5
psam 7/5	50	70	110				$1\times10^{+05}$	0.28	1.12×10^{-21}	4	$1\times10^{+05}$	0.26	1.12×10^{-21}	4					$3.0\times10^{+14}$	−12.5
psam 1/2	100	50	90				$1\times10^{+05}$	0.28	1.12×10^{-21}	4	$1\times10^{+05}$	0.26	1.12×10^{-21}	4					$3.0\times10^{+14}$	-25
psam 1/8	400	50	90				$1\times10^{+05}$	0.28	1.12×10^{-21}	4	$1\times10^{+05}$	0.26	1.12×10^{-21}	4					$3.0\times10^{+14}$	-100
pel = psam	50	50	90				$1\times10^{+05}$	0.28	1.12×10^{-21}	4	$1\times10^{+05}$	0.26	1.12×10^{-21}	4					$3.0\times10^{+14}$	−12.5
pel 5× weaker	50	50	90				$1\times10^{+05}$	0.28	1.12×10^{-21}	4	$1\times10^{+05}$	0.26	5.60×10^{-21}	4					$3.0\times10^{+14}$	−12.5
pel 10× weaker	50	50	90				$1\times10^{+05}$	0.28	1.12×10^{-21}	4	$1\times10^{+05}$	0.26	1.12×10^{-20}	4					$3.0\times10^{+14}$	−12.5
pel 100× weaker	50	30	90				$1\times10^{+05}$	0.28	1.12×10^{-21}	4	$1\times10^{+05}$	0.26	1.12×10^{-19}	4					$3.0\times10^{+14}$	−12.5
pel 1000× weaker	50	50	90				$1\times10^{+05}$	0.28	1.12×10^{-21}	4	$1\times10^{+05}$	0.26	1.12×10^{-18}	4					$3.0\times10^{+14}$	−12.5
n1	50	50	90				$1\times10^{+05}$	0.28	2.84×10^{-17}	1	$1\times10^{+05}$	0.26	2.84×10^{-17}	1					$3.0\times10^{+14}$	−12.5
n2	50	50	90				$1\times10^{+05}$	0.28	9.66×10^{-19}	2	$1\times10^{+05}$	0.26	9.66×10^{-19}	2					$3.0\times10^{+14}$	−12.5
n3	50	50	90				$1\times10^{+05}$	0.28	3.29×10^{-20}	3	$1\times10^{+05}$	0.26	3.29×10^{-20}	3					$3.0\times10^{+14}$	−12.5
n5	50	50	90				$1\times10^{+05}$	0.28	3.81×10^{-23}	5	$1\times10^{+05}$	0.26	3.81×10^{-23}	5					$3.0\times10^{+14}$	−12.5
n6	50	50	90				$1\times10^{+05}$	0.28	1.30×10^{-24}	6	$1\times10^{+05}$	0.26	1.30×10^{-24}	6					$3.0\times10^{+14}$	−12.5
n7	50	50	90				$1\times10^{+05}$	0.28	4.42×10^{-26}	7	$1\times10^{+05}$	0.26	4.42×10^{-26}	7					$3.0\times10^{+14}$	−12.5
psam = quartz	55	50	90	5	3.8	25	$1\times10^{+05}$	0.28	1.12×10^{-21}	4	$1\times10^{+05}$	0.26	5.60×10^{-21}	4	$1\times10^{+05}$	0.3	1.12×10^{-21}	4	$3.0\times10^{+14}$	−12.5
psam 10× weaker	55	50	90	5	3.8	25	$1\times10^{+05}$	0.28	1.12×10^{-20}	4	$1\times10^{+05}$	0.26	5.60×10^{-20}	4	$1\times10^{+05}$	0.3	1.12×10^{-21}	4	$3.0\times10^{+14}$	−12.5
psam 100× weaker	55	50	90	5	3.8	25	$1\times10^{+05}$	0.28	1.12×10^{-19}	4	$1\times10^{+05}$	0.26	5.60×10^{-19}	4	$1\times10^{+05}$	0.3	1.12×10^{-21}	4	$3.0\times10^{+14}$	−12.5
psam 1000× weaker	55	50	90	5	3.8	25	$1\times10^{+05}$	0.28	1.12×10^{-18}	4	$1\times10^{+05}$	0.26	5.60×10^{-18}	4	$1\times10^{+05}$	0.3	1.12×10^{-21}	4	$3.0\times10^{+14}$	−12.5
psam 10,000× weaker	55	50	90	5	3.8	25	$1\times10^{+05}$	0.28	1.12×10^{-17}	4	$1\times10^{+05}$	0.26	5.60×10^{-17}	4	$1\times10^{+05}$	0.3	1.12×10^{-21}	4	$3.0\times10^{+14}$	−12.5
psam 100,000× weaker	55	50	90	5	3.8	25	$1\times10^{+05}$	0.28	1.12×10^{-16}	4	$1\times10^{+05}$	0.26	5.60×10^{-16}	4	$1\times10^{+05}$	0.3	1.12×10^{-21}	4	$3.0\times10^{+14}$	−12.5
psam 1,000,000× weaker	55	50	90	5	3.8	25	$1\times10^{+05}$	0.28	1.12×10^{-15}	4	$1\times10^{+05}$	0.26	5.60×10^{-15}	4	$1\times10^{+05}$	0.3	1.12×10^{-21}	4	$3.0\times10^{+14}$	−12.5
psam 10× stronger	55	50	90	5	3.8	25	$1\times10^{+05}$	0.28	1.12×10^{-22}	4	$1\times10^{+05}$	0.26	5.60×10^{-22}	4	$1\times10^{+05}$	0.3	1.12×10^{-21}	4	$3.0\times10^{+14}$	−12.5
psam 100× stronger	55	50	90	5	3.8	25	$1\times10^{+05}$	0.28	1.12×10^{-23}	4	$1\times10^{+05}$	0.26	5.60×10^{-23}	4	$1\times10^{+05}$	0.3	1.12×10^{-21}	4	$3.0\times10^{+14}$	−12.5
psam 1000× stronger	55	50	90	5	3.8	25	$1\times10^{+05}$	0.28	1.12×10^{-24}	4	$1\times10^{+05}$	0.26	5.60×10^{-24}	4	$1\times10^{+05}$	0.3	1.12×10^{-21}	4	$3.0\times10^{+14}$	−12.5

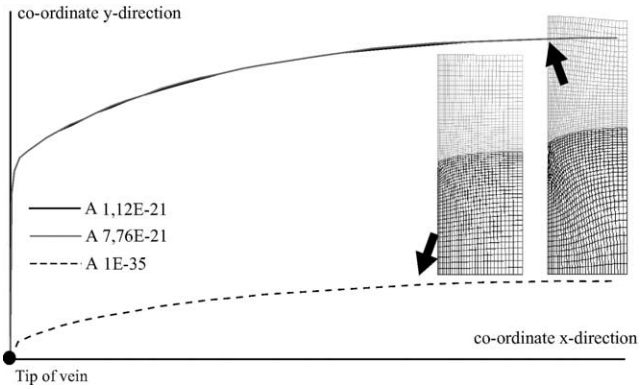

Fig. 6. Diagram showing half a mullion curve (pelite–psammite interface) for the calibration of model 1. The scale of the figure is 1/1. The input parameters of the simulations represented in this diagram are shown in Table 1.

including temperature, n the stress exponent, t the time and m the time exponent. As usual in geomechanical modelling, primary creep is neglected by setting m to zero. Under these conditions Eq. (2) reduces to Eq. (1) with $A = A_0 \exp^{(-Q/RT)} d^{-m}$.

The power-law creep in this model is volume constant and we assume no volume loss during deformation due to long-distance transport of material during pressure solution creep (Erslev and Ward, 1994).

3.3. History information

In each model the rate of deformation was approximated by the maximum time of mullion formation as suggested in the geological setting (~10 Ma). The model is shortened at a constant displacement rate during deformation. There is no information about possible changes in rate of deformation of the mullions, but we believe that small changes will not have a major effect on the results.

The aim of our modelling at this stage is to determine how different input parameters affect the stresses, strains and mullion morphology in the model. This will be used to evaluate the use of mullions as a gauge to constrain the in-situ rheological properties of psammite at the time of mullion formation (under low-grade metamorphic conditions).

4. Parameter sensitivity analysis

The following parameters are investigated:

1. Elastic versus creep deformation
2. Total shortening
3. Layer thickness of the psammite and pelite and the spacing of the veins
4. Competence contrast of the pelite and psammite
5. Stress exponent of the psammite
6. Competence contrast of the vein quartz and psammite.

The first part of the analysis (1–5) is performed using the rigid-vein model (model 1) in order to understand the basics of the model. After calibration, the model is extended to the model with a deformable vein (model 2) and more complex influences with respect to the quartz vein are examined (6). The input parameters of the different simulations used for this parameter sensitivity analysis are listed in Table 1. Numerical convergence of both models for all parameters was robust and stable.

4.1. Elastic versus creep deformation

As discussed above, the rigid-vein model consists of two materials (psammite and pelite). Since the material properties for both lithologies, to our knowledge, are not reported in literature, the starting point of the sensitivity analysis is the assumption that the psammite is the competent material with respect to pelite and therefore the rheology of wet quartz, as specified by Hirth et al. (2001), is used for psammite.

For the first two simulations using model 1, the whole grid has the properties of wet quartz (Hirth et al., 2001). At temperatures of 350–400 °C this corresponds to A-values ranging from 1.12×10^{-21} to 7.76×10^{-21}. These maximum and minimum values are represented in the simulations. We compare these simulations with a third one with an extremely low A-value of 1×10^{-35} (Fig. 6). This serves only to illustrate stresses in the model due to elastic deformation only. A similar Young's modulus (10^5 MPa) is used for all three materials while Poisson ratios of 0.26, 0.28 and 0.30 are taken for pelite, psammite and quartz, respectively. As expected, the elastic strain is much lower than creep strain in models 1.12×10^{-21} and 7.76×10^{-21} and the absolute values of the Young's modulus and Poisson ratio have very little effect on the results.

The deformed interface between psammite and pelite of the different simulations is shown in Fig. 6. It can be seen that the shape of mullions is similar for the simulations with A-values of 7.76×10^{-21} and 1.12×10^{-21}. Moreover, in both simulations, the deformation is dominated by creep. The elastic strain represents only 1–0.1% of the total strain (Fig. 7a). In contrast, the simulation with an extremely low A-value of 1×10^{-35} is dominated by elastic deformation (Fig. 7b) and produces a different shape of mullions. Here stresses are unrealistically high and vertical extension is much less (Figs. 6 and 7). Based on this, a value of $A = 1.12 \times 10^{-21}$ will be used as a reference for further analysis with model 1.

4.2. Shortening

The effect of the layer-parallel shortening on the rigid-vein model is illustrated in Fig. 8. Different shapes of

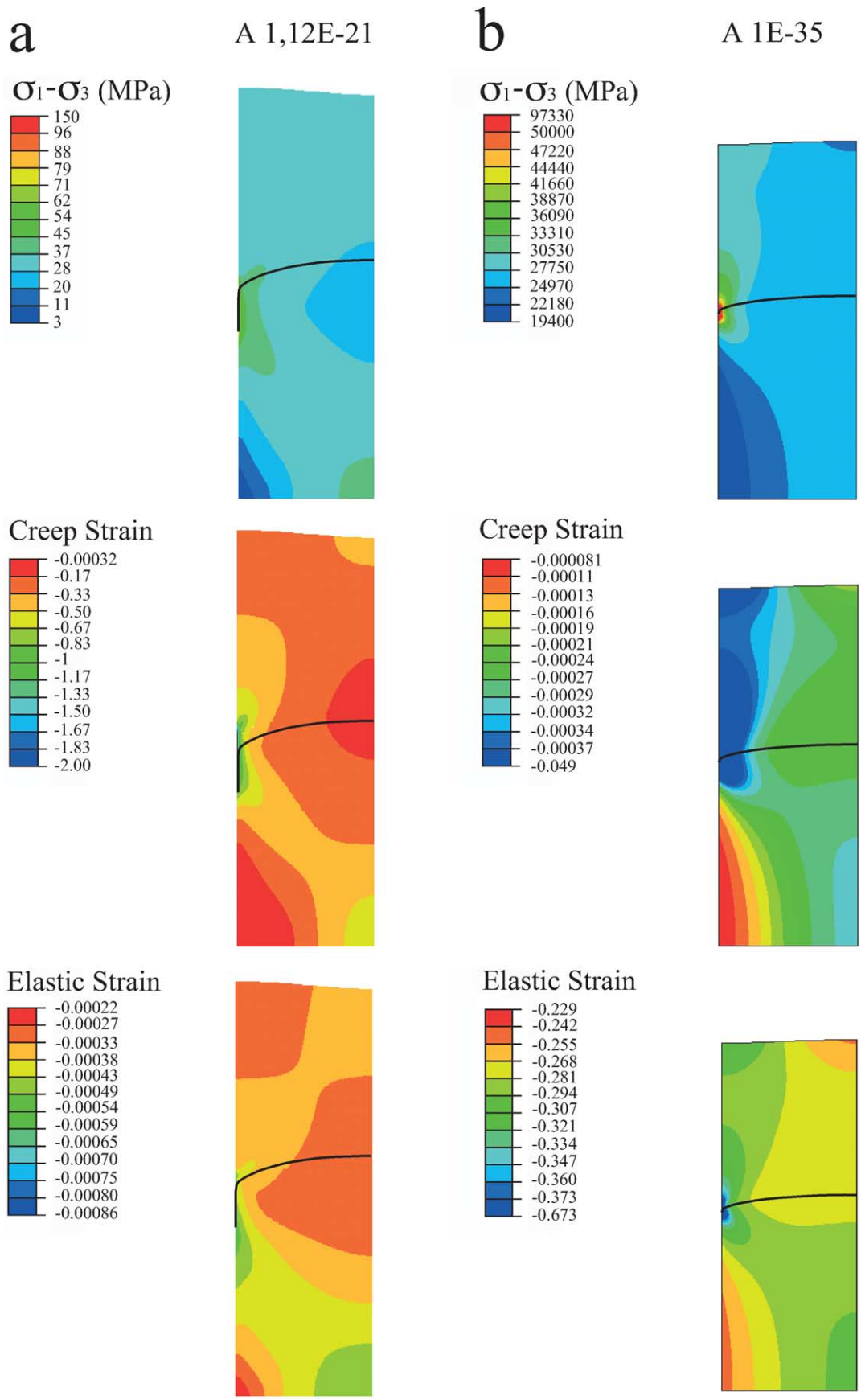

Fig. 7. Comparison of the differential stress, creep strain and elastic strain in simulations (a) 1.12×10^{-21} and (b) 1×10^{-35}. The black line represents the pelite–psammite interface.

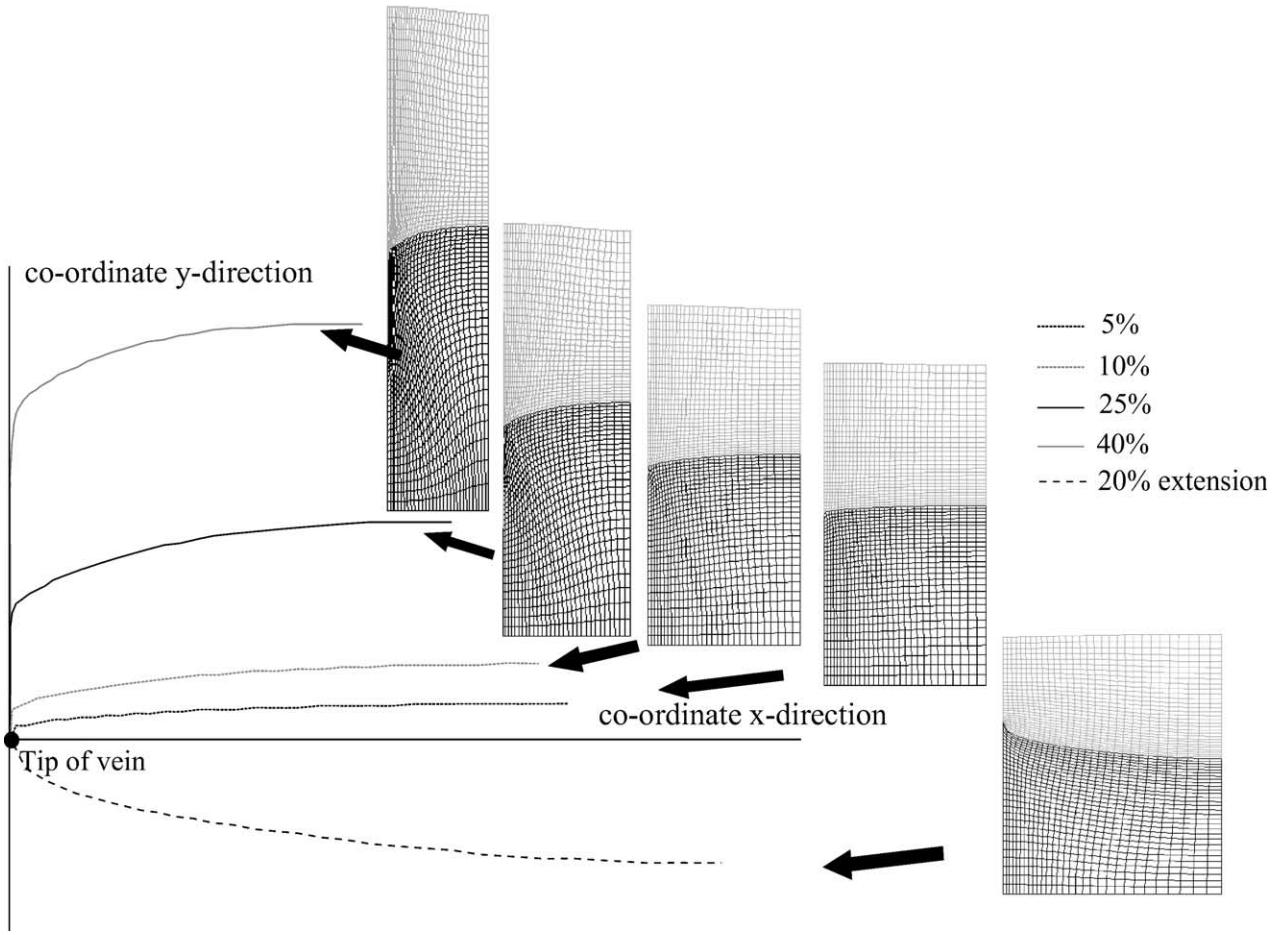

Fig. 8. Different degrees of shortening (2, 10, 25 and 40%) and extension (20% extension) of the geodynamic mullion model. Shortening of the model gives rise to the development of mullions while extension of the model gives rise to the development of bone-shaped structures. The input parameters of the different simulations represented are reported in Table 1. The scale of the diagram is 1/1.

mullion can be observed for a shortening of, respectively, 5, 10, 25 and 40%. The higher the degree of shortening, the more concentrated the strain becomes towards the tip of the vein and the more curved the lobe of the mullion becomes. The numerical problems of high strains are solved by using 4-node bilinear hybrid elements in the model. The dependence of the shape of mullions on the degree of shortening demonstrates the importance of constraining this parameter. Moreover, a simulation with 20% extension of the psammite grid is compared with the simulations with different degrees of shortening. As can be observed in Fig. 8, extension of the psammite grid gives rise to the development of 'bone-shaped' structures described by Ramsay (1982) and Malavieille and Lacassin (1988).

4.3. Layer thickness of the psammite and pelite and spacing between the veins

The layer thickness of the psammite and pelite and the spacing between the veins is represented by the aspect ratio of the undeformed mesh of both the psammite and pelite. These aspect ratios were varied with respect to the reference model to evaluate their effect on the shape of the mullions (Figs. 9 and 10; Table 1).

The aspect ratio of the psammites clearly is important for the final shape of the lobes of the mullion (Fig. 9) while the aspect ratio of the pelite has no influence (Fig. 10). The dependence of the shape of the mullion on the aspect ratio of the psammite segments shows that the wider the vein spacing with respect to the layer thickness of the psammite the less pronounced the buckling will be at the contact with the vein. Field observations corroborate this result (Fig. 11).

4.4. Strain

Microscopically, the deformed vein quartz shows evidence of plastic deformation, with subgrain formation and incipient recrystallisation (Fig. 12; Urai et al., 2001; Kenis et al., 2002). Based on the extent of dynamic recrystallisation of the vein quartz, we use an extension of the veins of 5–10% for this analysis (Urai et al., 1986), keeping in mind that this varies in nature, as shown, e.g. by boudinaged intra-mullion veins (Kenis et al., 2002).

Results show that the initial ratio between vein spacing–

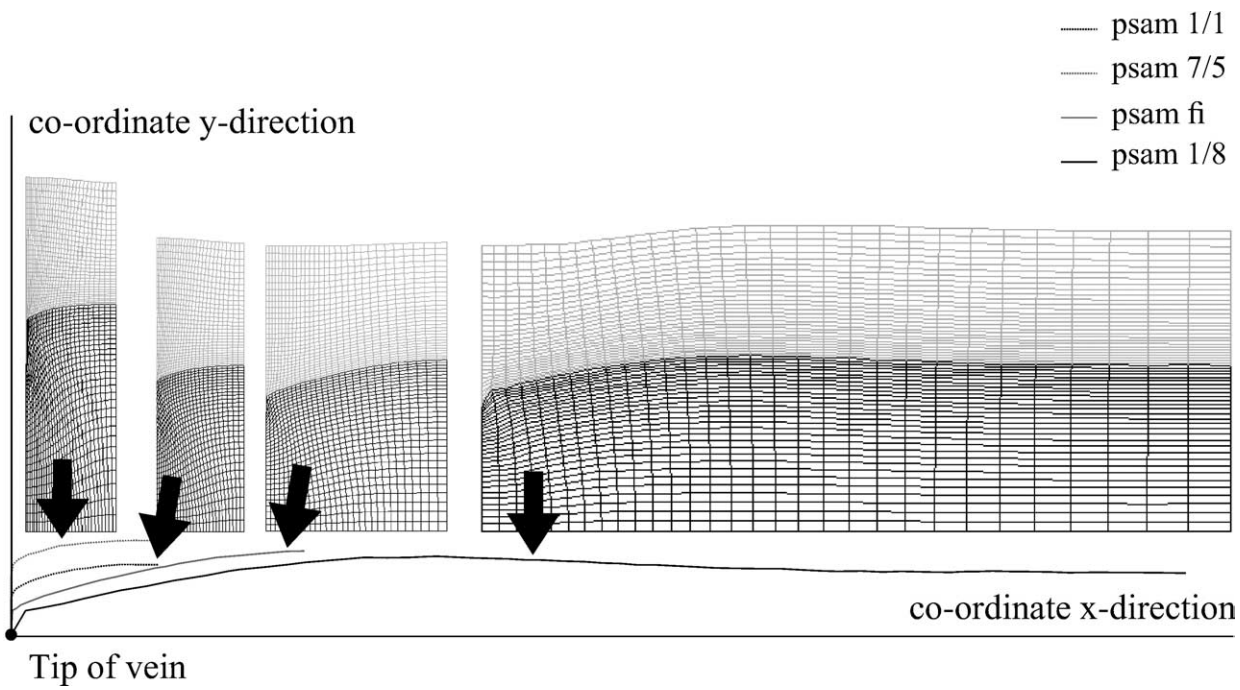

Fig. 9. Diagram showing the influence of the aspect ratio of the psammite segment between the veins. The scale of the figure is 1/1. The input parameters of models represented in this diagram are shown in Table 1. psam 1/1, 7/5, 1/2 and 1/8 refer to an initial aspect-ratio (height/width) of the psammite segments of 1/1, 7/5, 1/2 and 1/8, respectively.

layer thickness and the horizontal shortening are controlling parameters on the shape of the mullions. Therefore, to estimate these parameters, we reconstructed the initial shape of a number of mullions assuming no volume change and plane strain (Fig. 13). Thus, the area of psammite between two veins is converted to a rectangle with thickness equal to 95% of the length of the vein (to correct for deformation of the vein). For mullions investigated in the field (Table 2) this gives a layer-parallel shortening of the psammite layers between 18 and 32%. Based on this, we run the simulation in the next part of the paper to 25% layer-parallel shortening.

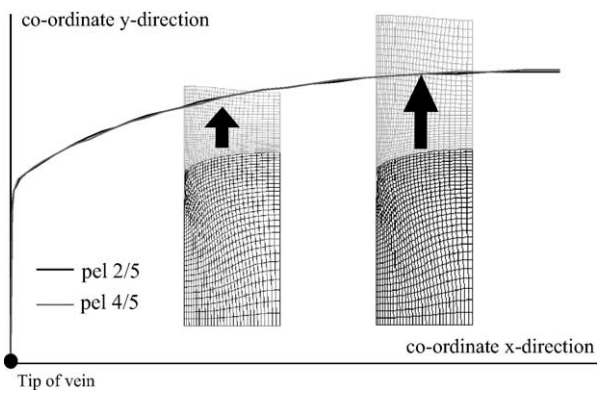

Fig. 10. Diagram showing the influence of the aspect ratio of the pelite. The scale of the figure is 1/1. The input-parameters of the simulation are represented in Table 1. pel 2/5 and 4/5 refer to an initial aspect-ratio (height/width) of the pelite of 2/5 and 4/5, respectively.

4.5. Competence contrast of psammite and pelite

In order to investigate the effect of the competence contrast of psammite and pelite, the *A*-value of pelite was increased stepwise while keeping the *A*-value of psammite constant (Fig. 14; Table 1). Keeping the values of the stress exponent and the strain rate constant for all simulations in Fig. 14, the increase directly corresponds to a reduction in competence.

Results of the different simulations show only a small effect of this competence contrast on the shape of a mullion. Once the competence contrast exceeds the value of five, the effect completely disappears. From literature, realistic viscosity contrasts of quartzite relative to pelite are estimated to be less than 10–5 (Treagus, 1999, 2002;

Table 2
Table showing the estimated shortening percentage for psammite of mullions at different localities by means of a volume retaining strain analysis and strain of quartz of 5%

Sample	Stretching percentage of ~5%
Boeur1	17.9–20.4
Boeur2	28.4
Boeur6	24.3
Slr1	26.5–25.4
Slr2	29.5
Slr3	32.3
Mardas2	28
Mardas3	23.1
Rouette	28.2–26.7
Bertix1	19.8

Fig. 11. Mullions in the Bastogne area (Carrière Mardasson) showing a large aspect ratio (height/width; pencil = 15 cm) (a). The curve of the mullion is less pronounced than mullions with a smaller aspect ratio for the psammite segments (hammer = 35 cm) (b).

Treagus and Treagus, 2002). Since the competence contrast between pelite and psammite has almost no influence on the shape of a mullion, we conclude that the effect of the rheology of the pelites on the shape of a mullion is negligible.

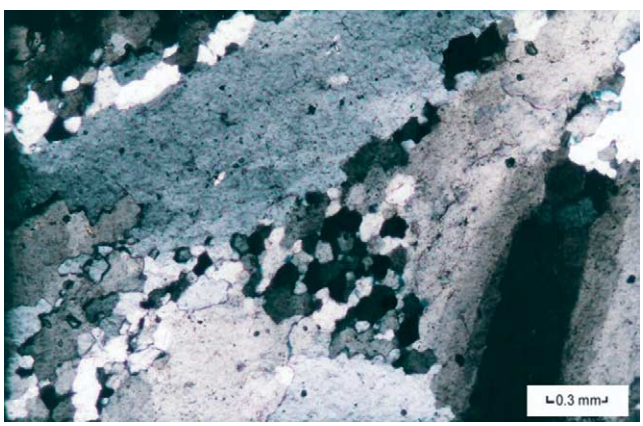

Fig. 12. Picture of vein quartz showing relics of old quartz grains, which pass into domains of recrystallised grains (scale bar = 0.3 mm).

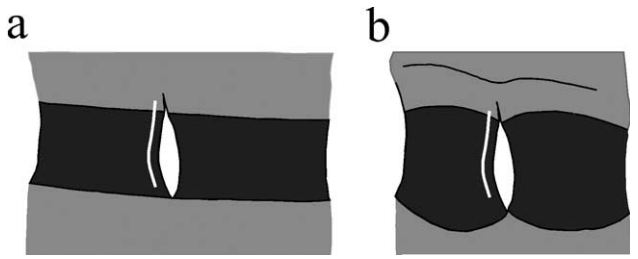

Fig. 13. Volume retaining strain analysis of mullion showing (a) the aspect ratio of the psammite segment before mullion formation and (b) after mullion formation. Dark grey parts of schematic drawing represent psammite, light grey represents pelite and white represents quartz.

4.6. Stress exponent

Now we examine the influence of the stress exponent of the psammite on the shape of the mullion (Table 1). To make sure that the competence of the competent material remains similar for all simulations, the equation $\delta\epsilon/\delta t = A(\sigma_1 - \sigma_3)^n$ was used to calculate corresponding A-values (Fig. 15). Starting with the power law for wet quartz (Hirth et al., 2001), a shortening of 25% in 10 Ma, as suggested by the geological constraints, we calculate a differential stress of ~30 MPa in the psammite in the reference simulation.

The results of the simulations using model 1 confirm that the expected shape of the mullion is a strong function of the stress exponent n of psammite (Fig. 16). For linear viscous materials ($n = 1$) the curvature is relatively continuous while for increasing values of n ($n > 1$) the curvature increases towards the position of the vein.

From the results it is clear that the difference in curvature between $n = 1$ and $n = 3$ is bigger than the difference between e.g. $n = 4$ and $n = 6$. Fig. 17 demonstrates that the differential stress in the different simulations is of the same order of magnitude.

4.7. Competence contrast of vein quartz and psammite

The next step in the parameter sensitivity analysis

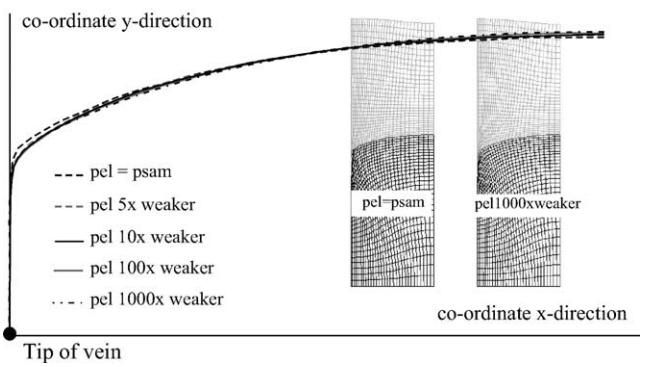

Fig. 14. Diagram showing the influence of the difference in competence between the psammite and pelite. The scale of the figure is 1/1. The input parameters of the simulation are represented in Table 1. Pel = psam—pelite has the same competence as the psammite; pel 5 × weaker—pelite is 5 × weaker than the psammite; etc.

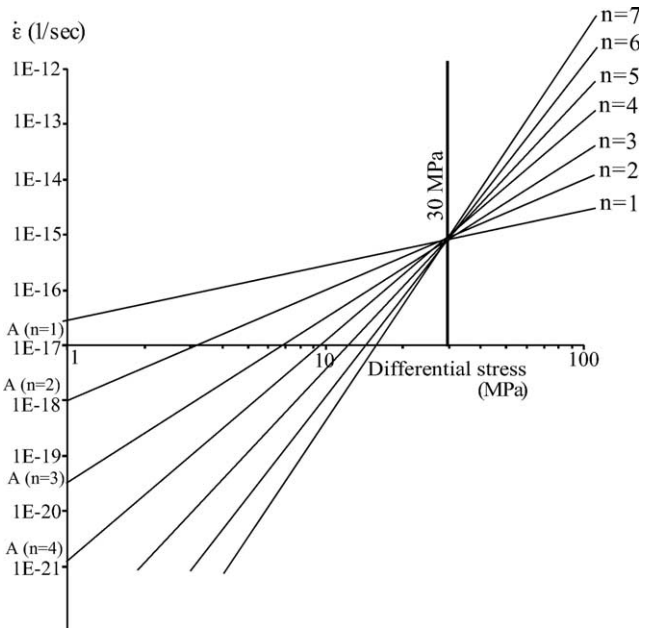

Fig. 15. Diagram showing the recalculation of A for different n values at differential stresses of ~30 MPa and strain-rates of $\sim 8 \times 10^{-16}\ s^{-1}$.

involves the competence contrast of vein quartz and psammite, for which model 2 is used. For a total rigid quartz vein, the results of models 1 and 2 are indistinguishable.

In this model the vein quartz is the most competent material and is assigned the wet-quartz rheology of Hirth et al. (2001) deforming at temperatures of 350–400 °C. Wet quartz is an appropriate choice based on the large amount of aqueous fluid inclusions present in the vein quartz as demonstrated by Darimont et al. (1988) and Kenis et al. (2002). As previously discussed, the time of shortening of the model is 3×10^{14} s (~10 Ma) and the degree of shortening of the mullions is 25%. A competence contrast of psammite/pelite of five is retained for all the simulations (cf. Treagus, 1999, 2000).

To evaluate the competence contrast of vein quartz and psammite, a stress exponent of four (Hirth et al., 2001) was used for all materials and only A-values have been varied to reflect a difference in competence.

The results show that the shape of the mullion is a strong function of the competence contrast of vein quartz versus psammite (Fig. 18; Table 1). At very high competence contrast the deformation of the quartz vein becomes zero and the model is reduced to the rigid-vein model (Figs. 18 and 19). With decreasing competence contrast, the deformation of the psammite and quartz becomes more and more similar, evolving to homogeneous flattening at a competence ratio of one (Fig. 18). When the competence contrast is reversed, deformation in the vein quartz becomes more than in the psammite and inverted mullions are formed (Figs. 18–20).

Keeping account of the geometry of the mullions in the field, the parameter sensitivity analysis is indicative of a

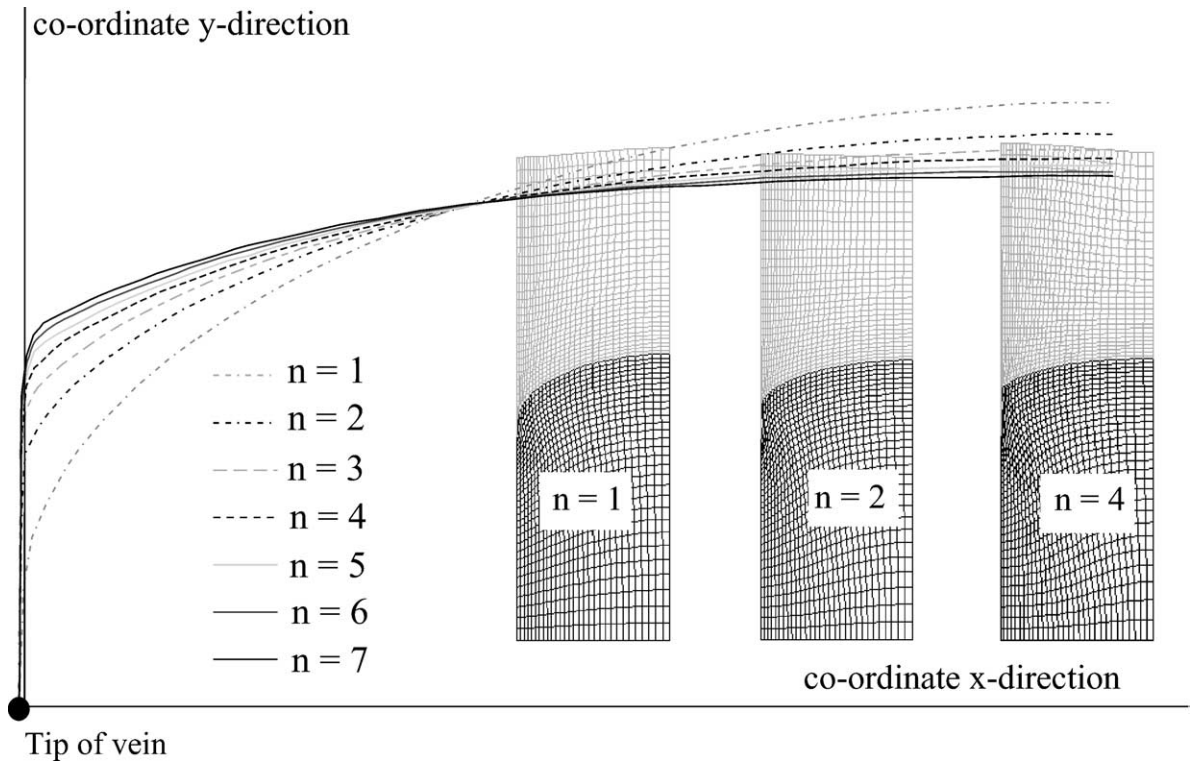

Fig. 16. Diagram showing the influence of the stress exponent of the power law of psammite. The scale of the figure is 1/1. The input parameters of the simulations are represented in Table 1.

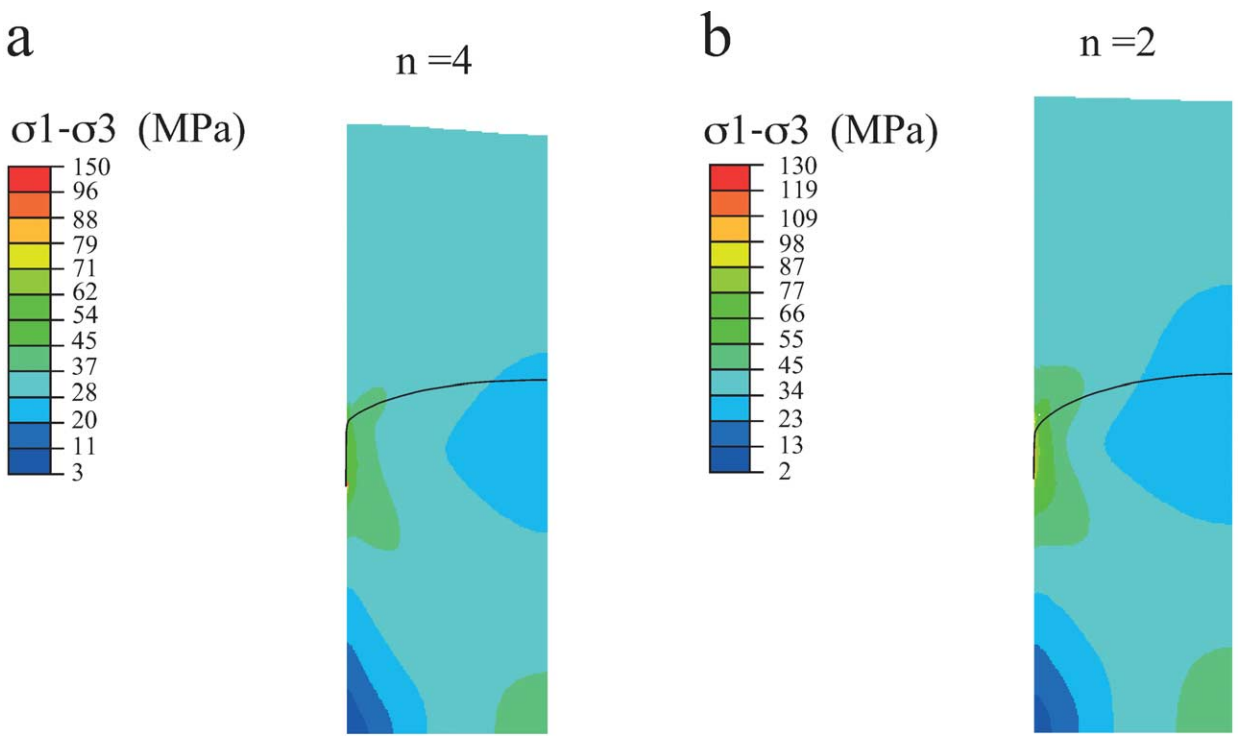

Fig. 17. Differential stress in the simulations where the stress exponent of the power law for psammite is (a) 4 and (b) 2. The legend shows that the stress is in the same order of magnitude for both simulations.

relatively large difference in competence (and thus strain) between the psammite and quartz at the time of mullion formation (Figs. 18 and 20). This suggestion is based on the pronounced shape of the mullions in the field, which would have been absent if the competence of the quartz and psammites was similar during layer-parallel shortening (Fig. 20).

This pronounced shape is the consequence of a relatively large difference in strain between the psammite and vein quartz resulting in a large difference in strain rate. This difference in strain rate is due to a competence contrast, which promotes strain partitioning between compositional bands (cf. Ramsay and Lisle, 2000). In the case of the mullions, the pelite is

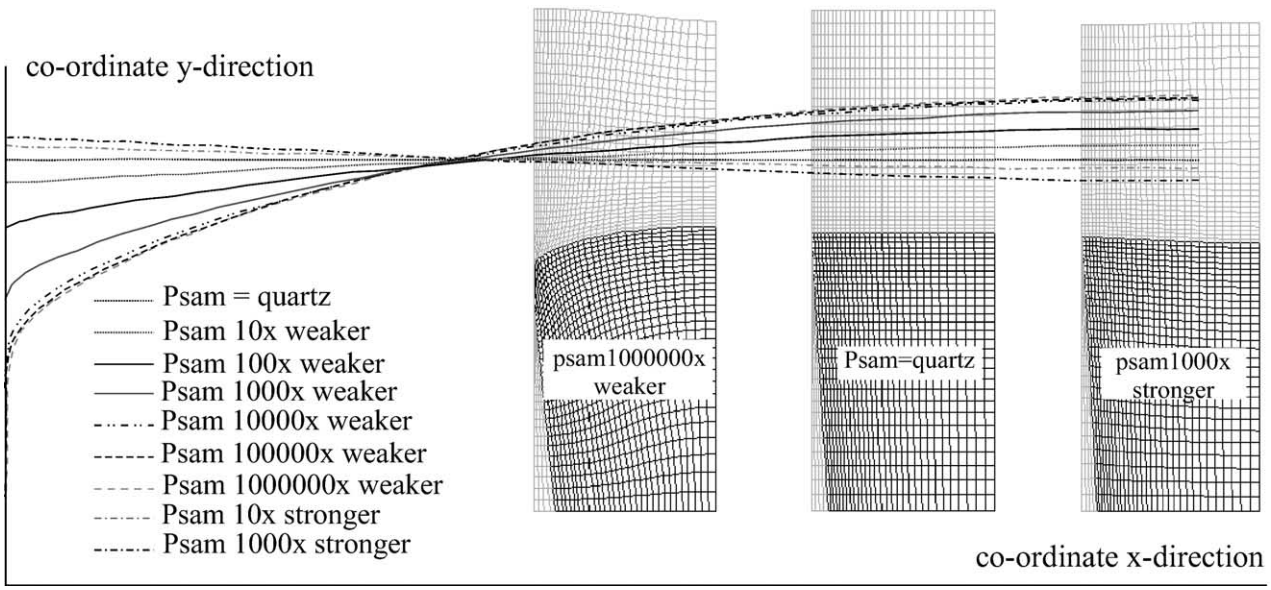

Fig. 18. Diagram showing the influence of the difference in competence between the psammites and quartz. The scale of the figure is 1/1. The input parameters of simulations are represented in Table 1. psam = quartz—psammite has the same strength as the quartz; psam 10 × weaker—psammite is 10 × weaker than the quartz; etc.

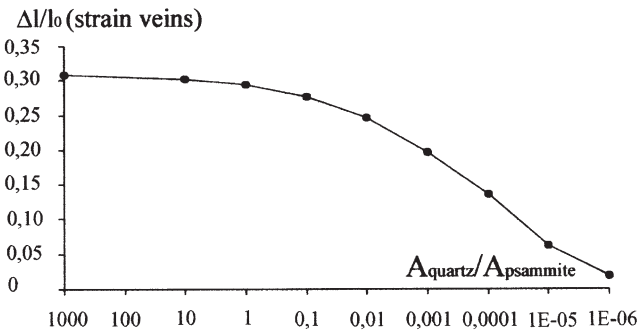

Fig. 19. Diagram representing the difference in strain of the vein corresponding to different competence ratios vein quartz/psammite. The more competent the quartz becomes with respect to the psammite the more model 2 reduces to the rigid vein model (model 1) with the strain in the vein quartz equal to zero.

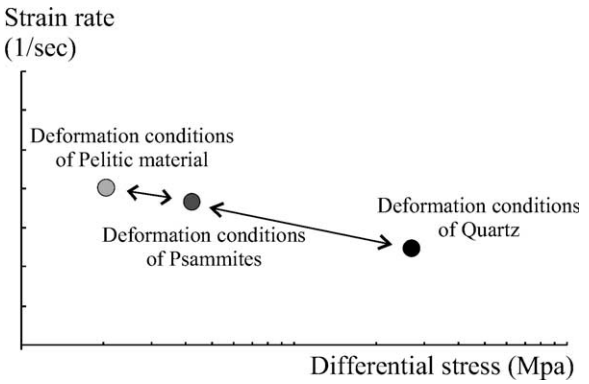

Fig. 21. Schematic representation of the relationship of the deformation conditions of the different lithologies of the mullions at the time of mullion development with quartz stronger than psammite stronger than pelite.

incompetent with respect to the psammite, while the psammite in its turn is less competent with respect to the vein quartz. This suggests that during the development of the mullions the strain, and thus also the strain rate, was higher for the pelite than for the psammite, than for the vein quartz (Fig. 21). This statement is corroborated by the predicted strain for quartz and psammites in the mullions. The first one is estimated to range from 5 to 10% while the second ranges from 18 to 32%. Additionally, the total strain due to the Variscan shortening for the pelite in the High-Ardenne Slate Belt is estimated at a minimum of 50% by means of X-ray pole figure goniometry.

5. Discussion

Based on our parameter sensitivity analysis, four main controlling parameters were identified for the development of the specific shape of mullions:

1. Total shortening
2. Initial shape of the psammite segments
3. Stress exponent of the psammite
4. Competence contrast vein quartz versus psammite.

On the one hand, the dependence of the shape of the

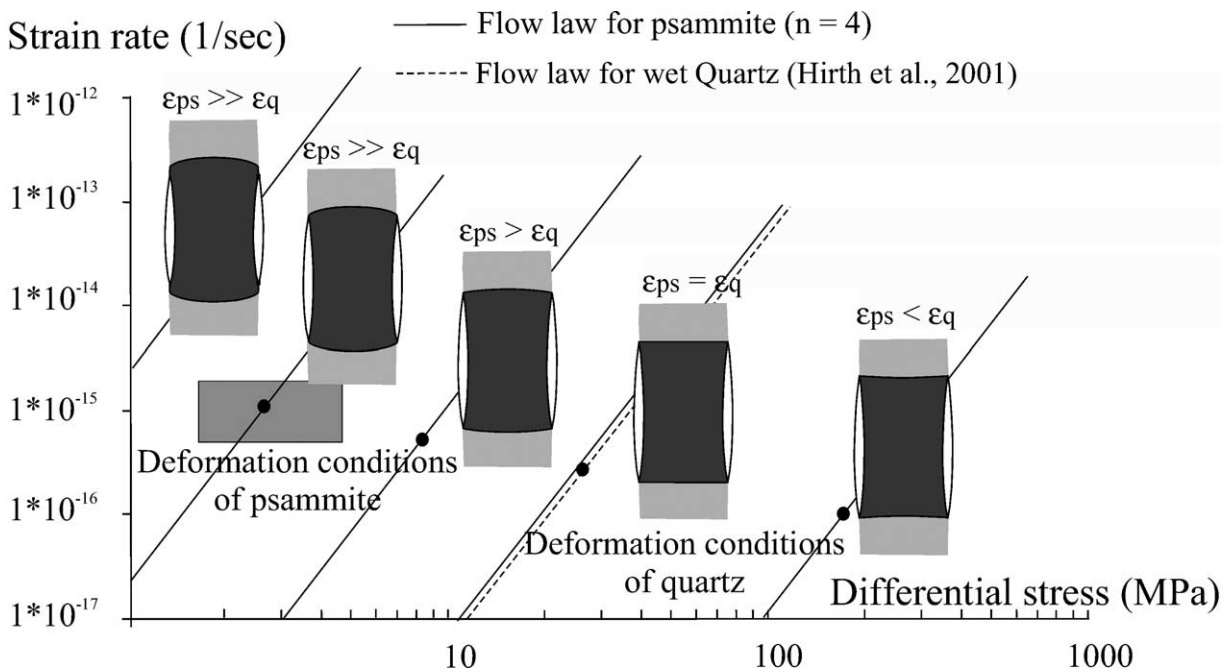

Fig. 20. Schematic representation of Fig. 18 showing the influence of the difference in competence between psammites and quartz on the shape of the mullions. The full lines correspond to different flow laws for psammite while the dashed line corresponds to the flow law for wet quartz deforming at temperatures of 350–400 °C according to Hirth et al. (2001). The grey box in the diagram represents the estimated competence of psammite with respect to that of quartz in order to develop the pronounced shape of the mullions. Here the strain of the vein quartz is larger than zero but considerably less than that of psammite.

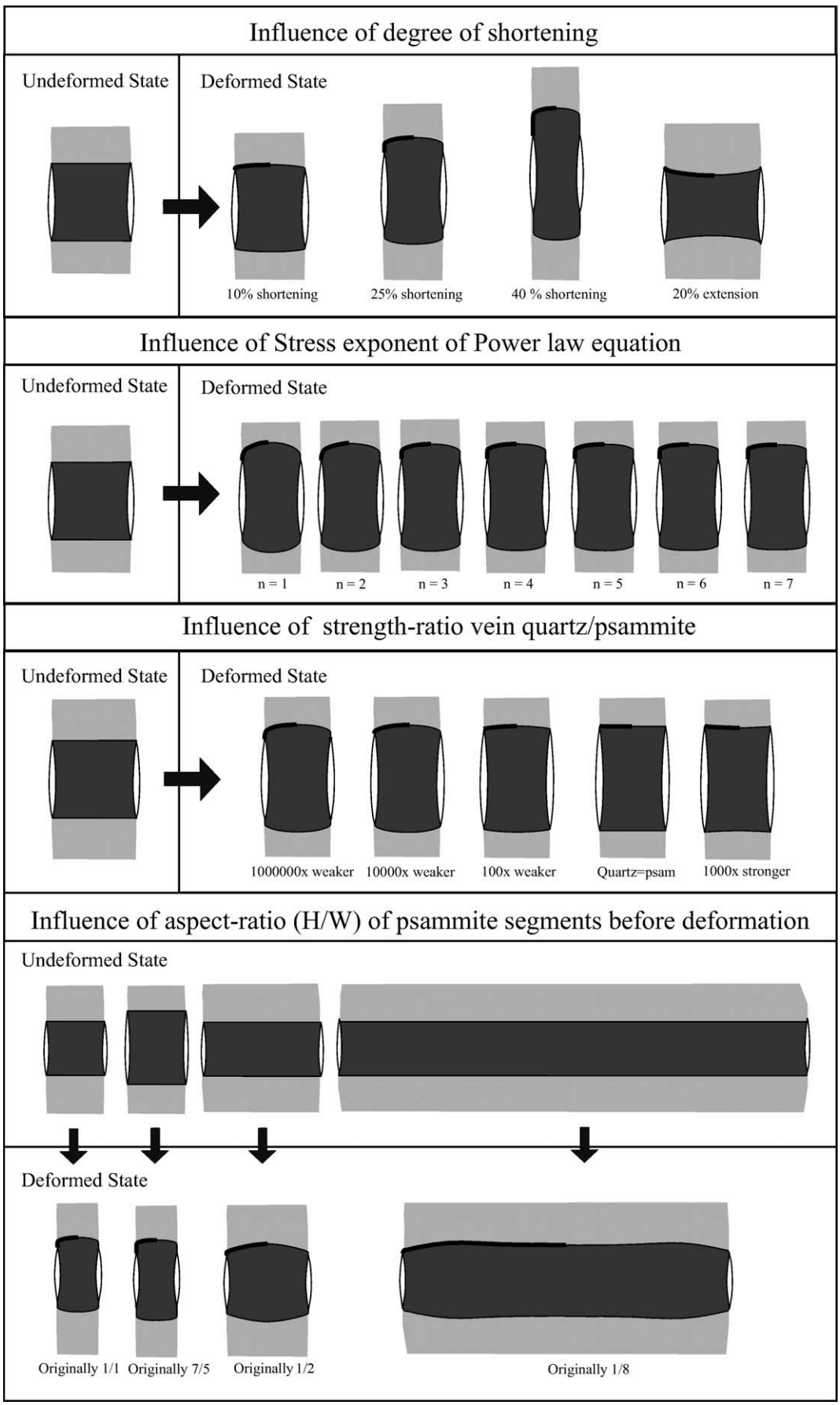
Influence of degree of shortening
Undeformed State
Deformed State
10% shortening
25% shortening
40 % shortening
20% extension
Influence of Stress exponent of Power law equation
Undeformed State
Deformed State
n = 1
n = 2
n = 3
n = 4
n = 5
n = 6
n = 7
Influence of strength-ratio vein quartz/psammite
Undeformed State
Deformed State
1000000x weaker
10000x weaker
100x weaker
Quartz=psam
1000x stronger
Influence of aspect-ratio (H/W) of psammite segments before deformation
Undeformed State
Deformed State
Originally 1/1
Originally 7/5
Originally 1/2
Originally 1/8

mullions on the competence contrast vein quartz versus psammite is represented by the difference in *A*-value of the power-law of quartz and psammite in the numerical simulation. This difference reflects a difference in competence and thus a difference in strain between both lithologies (Figs. 19 and 22). On the other hand, the *n*-value of the power law for psammite is a matter of curvature of the mullions (Fig. 22). Thus for a given initial configuration (layer thickness and vein spacing) the morphology of the mullions and the distribution of strain is a strong function of the rheological parameters (*A* and *n*) of psammite and thus a potential gauge for paleorheology.

A possible method to determine the rheological parameters (*A* and *n*) would start with a digitised geometry of an individual mullion, which is used to quantify the first two controlling parameters (1 and 2) by means of a volume-retaining strain analysis (Fig. 13). Then, keeping in mind a number of constraints determined by microstructural analysis, to determine stress and strain in the vein, a finite element model would be sought for which the difference between all measured and calculated parameters are minimised. If, in addition, one can show that there is only one combination of input parameters for which this is the case, this would yield values of *A* and *n* of psammites deforming in nature under greenschist facies conditions. Results of such a case study are presented in a follow-up paper (Kenis et al., 2004, submitted).

Next to the development of mullions due to layer-parallel shortening, the numerical model is capable of modelling the development of other layer-parallel deformation structures with layer-perpendicular veins such as 'bone-shaped' structures (e.g. dogbones, inverted mullions). These structures occur worldwide and in different geological settings. Therefore, the applicability of the numerical model to all layer-parallel shortening/extension structures with pre-existing layer-perpendicular veins creates future perspective for the use of the model as a paleorheological gauge.

6. Conclusion

A parameter sensitivity analysis has been performed on the geomechanical mullion model using the ABAQUS package in order to qualify the controlling parameters on the development of the specific shape of mullions (Fig. 22). On the one hand, the parameter sensitivity analysis shows that the competence contrast between psammite and pelite and the dimension of the pelite before deformation are of relatively no importance for the shape of mullions. On the other hand, the analysis confirmed the hypothesis that the stress exponent of the psammite is an important determining parameter for the shape of mullions. Moreover, it is demonstrated that, in addition to the stress exponent, the degree of shortening of the psammite segments, their initial aspect ratio and the competence contrast between vein quartz and psammite are also important controlling parameters.

Taking into account the effect of the *n*-value of the psammite and the competence contrast of vein quartz versus psammite, it was found that the specific geometry of the mullions is a strong function of the rheological parameters of psammite and thus a suitable gauge for paleorheology. Given the capacity of the mullion model to perform deformation at realistic geological conditions the technique provides a good tool to determine the in-situ rheology of psammite in slate belts under low-grade metamorphic conditions. Moreover, the parameter sensitivity analysis illustrates the range of layer-parallel shortening/extension structures associated with layer-perpendicular quartz veins that can be expected in nature (e.g. dogbones, inverted mullions) and creates a future perspective for the use of the model as a paleorheological gauge for these structures.

Acknowledgements

We thank Susan Treagus and Yves Leroy for their helpful and constructive reviews and Cees Passchier for editing the manuscript. Manuel Sintubin is a Research Associate of the Onderzoeksfonds-K.U.Leuven. We would also like to thank Bert Vanbael, Shen He and Rudi Vanlaer for their help and discussions at MTM.

References

Ahrendt, H., Clauer, N., Hunziker, J., Weber, K., 1983. In: Martin, H., Eder, F.W. (Eds.), Intercontinental Fold Belts. Case Studies in the Variscan Belt of Europe and the Damara Belt in Namibia, Springer, Berlin, pp. 323–338.

Beugnies, A., 1983. Structure de l'aire anticlinale de l'Ardenne à l'Ouest du méridien de Libramont. Annales de la Société géologique du Nord 104, 165–173.

Biot, M.A., 1961. Theory of folding of stratified viscoelastic media and its implications in tectonics and orogenesis. Geological Society of America Bulletin 72, 1595–1631.

Bos, B., Spiers, C.J., 2002. Frictional-viscous flow in phyllosilicate-bearing fault rock: microphysical model and implications for crustal strength profiles. Journal of Geophysical Research 107(B2), 101029.

Burov, E.B., 2003. Discussion: the upper crust is softer than dry quartzite. Tectonophysics 361, 321–326.

Cattin, R., Avouac, J.P., 2000. Modelling mountain building and the seismic cycle in the Himalaya of Nepal. Journal of Geophysical Research 105, 13389–13407.

Darimont, A., Burke, E., Touret, J., 1988. Nitrogin-rich metamorphic fluids in Devonian metasediments from Bastogne, Belgium. Bulletin Minéral. 111, 321–330.

Fig. 22. Schematic drawing showing the influence of the four main controlling parameters on the shape of the mullions. All mullion drawings are on the scale of 1/1.

Erslev, E.A., Ward, D.J., 1994. Non-volatile element and volume flux in coalesced slaty cleavage. Journal of Structural Geology 16(4), 531–553.

Fielitz, W., Mansy, J.-L., 1999. Pre- and synorogenic burial metamorphism in the Ardenne and neighbouring areas (Rhenohercynian zone, central European Variscides). In: Sintubin, M., Vandycke, S., Camelbeeck, T. (Eds.), Palaezozoic to Recent Tectonics in the NW European Variscan Front Zone. Tectonophysics 309, pp. 227–256.

Fletcher, R.C., 1995. Three-dimensional folding and necking of a power-law layer: are folds cylindrical, and, if so, do we understand why? Tectonophysics 247, 65–83.

Gleason, G.C., Tullis, J., 1995. A flow law for dislocation creep of quartz aggregates determined with the molten salt cell. Tectonophysics 247, 1–23.

Goffette, O., Liégeois, J.-P., André, L., 1991. Ae U–Pb dévonien moyen à supérieur des zircons du magmatisme bimodal du Massif de Rocroi (Ardenne, France): implications géodynamiques. Comptes Rendus de l'Académie des Sciences, Paris 312, 1155–1161.

Heard, H.C., Carter, N.L., 1968. Experimentally induced "natural" intragranular flow in quartz and quartzite. American Journal of Science 266, 1–42.

Hibbitt, H.D., Karlsson, B.I., Sorensen, E.P., 2002. ABAQUS/Standard User's Manual (Version 6.2). Pawtucket, RI.

Hirth, G., Teyssier, C., Dunlap, J., 2001. An evaluation of quartzite flow laws based on comparison between experimentally and naturally deformed rocks. International Journal of Earth Science 90, 77–87.

Jackson, J., 2002. Strength of the continental lithosphere: time to abandon the jelly sandwich? GSA Today September, 4–9.

Jaoul, O., 1984. Sodium weakening of Heavitree Quartzite: preliminary results. Journal of Geophysical Research 89, 4272–4280.

Jaoul, O., Tullis, J., Kronenberg, A., 1984. The effect of varying water content on the creep behavior of Heavitree quartzite. Journal of Geophysical Research 89, 4298–4312.

Kenis, I., Sintubin, M., Muchez, Ph., Burke, E.A.J., 2002. The 'boudinage' question in the High-Ardenne Slate Belt (Belgium): a combined structural and fluid-inclusion approach. Tectonophysics 348, 93–110.

Kenis, I., Urai, J.L., van der Zee, W., Hilgers, Ch., 2004. Rheology of fine grained rocks deforming in the middle crust. Submitted to Science.

Koch, P.S., Christie, J.M., Ord, A., George, R.P. Jr, 1989. Effect of water on the rheology of experimentally deformed quartzite. Journal of Geophysical Research 94, 13975–13996.

Kohlstedt, D.L., Evans, B., Mackwell, S.J., 1995. Strength of the lithosphere constraints imposed by laboratory experiments. Journal of Geophysical Research 100, 17587–17602.

Kramm, U., Buhl, D., 1985. U–Pb zircon dating of the Hill tonalite, Venn–Stavelot-Massif, Ardennes. Neues Jahrbuch für Geologie und Paläontologie Abhandelungen 171, 329–337.

Kronenberg, A.K., Tullis, J., 1984. Flow strengths of quartz aggregates: grain size and pressure effects due to hydrolitic weakening. Journal of Geophysical Research 89, 428–4297.

Lohest, M., Stainier, X., Fourmarier, P., 1908. Compte rendu de la session extraordinaire de la Société Géologique de Belgique, tenue à Eupen et à Bastogne les 29, 30 et 31 Août et le 1, 2 et 3 septembre 1908. Annales de la Sociéte Géologique Belge 35, 351–434.

Luan, F.C., Paterson, M.S., 1992. Preparation and deformation of synthetic aggregates of quartz. Journal of Geophysical Research 97, 301–320.

Malavieille, J., Lacassin, R., 1988. Bone-shaped boudins in progressive shearing. Journal of Structural Geology 10, 335–345.

Oncken, O., von Winterfeld, C., Dittmar, U., 1999. Accretion of a rifted passive margin: the Late Palaeozoic Rhenohercynian fold and thrust belt (Middle European Variscides). Tectonics 18, 75–91.

Oncken, O., Plesch, A., Weber, J., Ricken, W., Schrader, S., 2000. In: Franke, W., Haak, V., Oncken, O., Tanner, D. (Eds.), Orogenic Processes: Quantification and Modelling in the Variscan Belt, Geological Society, London, pp. 199–216.

Parrish, D.K., Krivz, A.L., Carter, N.L., 1976. Finite-element folds of similar geometry. Tectonophysics 32, 183–207.

Paterson, M.S., Luan, F.C., 1990. Quartzite rheology under geological conditions. In: Knipe, R.J., Rutter, E.H. (Eds.), Deformation Mechanisms, Rheology and Tectonics. Geological Society Special Publication 54, pp. 299–307.

Ramsay, J.G., 1982. Rock ductility and its influence on the development of tectonic structures in mountain belts. In: Hsu, K.J., (Ed.), Mountain Building Processes, Academic Press, London, pp. 111–127.

Ramsay, J.G., Lisle, R.J., 2000. The Techniques of Modern Structural Geology. Volume 3: Applications of Continuum Mechanics in Structural Geology, Academic Press, London.

Ranalli, G., 2003. Discussion: how soft is the crust? Tectonophysics 361, 319–320.

Shelton, G., Tullis, J., 1981. Experimental flow laws for crustal rocks. EOS, Translations of the AGU 62, 396.

Talbot, C.J., 1999. Can field data contain rock viscosities? Journal of Structural Geology 21, 949–957.

Timoshenko, S.P., Goodier, J.N., 1970. Theory of Elasticity, McGraw-Hill.

Treagus, S.H., 1983. A theory of finite strain variation through contrasting layers and its bearing on cleavage refraction. Journal of Structural Geology 5, 351–368.

Treagus, S.H., 1988. Strain refraction in layered systems. Journal of Structural Geology 10, 517–527.

Treagus, S.H., 1999. Are viscosity ratios of rocks measurable from cleavage refraction? Journal of Structural Geology 20, 895–901.

Treagus, S.H., 2002. Modelling the bulk viscosity of two-phase mixtures in terms of clast shape. Journal of Structural Geology 24, 57–76.

Treagus, S.H., Treagus, J.E., 2002. Studies of strain and rheology of conglomerates. Journal of Structural Geology 24, 1541–1567.

Urai, J.L., Means, W.D.M., Lister, G.S., 1986. Dynamic recrystallization of minerals. American Geophysical Union, Geophysical Monograph (the Paterson volume) 36, 161–199.

Urai, J.L., Spaeth, G., van der Zee, W., Hilgers, C., 2001. Evolution of mullion (formerly boudin) structures in the Variscan of the Ardennes and Eifel. Journal of the Virtual Explorer 3, 1–15.url: http://virtualexplorer.com.au/2001/Volume3review/Urai2/index.html.

Verhaert, G., 2001. Kwartsaders en dubbelzijdige mullions in de Lochkoviaanmetasedimenten in de Hoge-Ardennenleisteengordel (Groeve La Flèche, Bertrix, België). Unpublished Graduate Thesis. Katholieke Universiteit Leuven.

Weertman, H., 1968. Dislocation climb theory of steady-state creep. Translations of the ASME 61, 681–694.